ADVANCES IN GEOMATICS

VOLUME 01 • ISSUE 01 • OCTOBER 2023
e-ISSN: 3023-4980

ORIGINAL ARTICLE

Submission: 03/08/2023
Accepted: 18/09/2023

MODELING OF SEA LEVEL CHANGES WITH GNSS-IR METHOD AND COMPARATIVE ANALYSIS WITH TIDE GAUGE DATA

Gülşen YALÇİN[1*]

[1] Department of Geomatics, Kocaeli University, Kocaeli, Türkiye.

* Corresponding Author: G. Yalçin, gulsenyal03@gmail.com

ABSTRACT

The Global Navigation Satellite Systems Interferometric Reflectometry (GNSS-IR) method has emerged as a promising approach to analyzing reflected signals from various surfaces, providing valuable insights into the properties of reflection surfaces. By harnessing the capabilities of GNSS-IR, changes in sea level can be accurately determined when GNSS stations located in proximity to the sea possess a suitable viewing angle for receiving reflections from the sea surface. In this study, we conducted an extensive analysis of sea level changes using satellite data obtained from the MERS station, which is part of the Turkish National Permanent GNSS Network-Active (TUSAGA-Aktif) network, in the year 2021. Throughout the analysis process, we carefully considered the appropriate satellite elevation and azimuth angles, accounted for background conditions, applied dominant frequency limits, and employed minimum-maximum frequency filtering techniques. We evaluated the data using 16 distinct analysis strategies and verified the sea level measurements against the Erdemli Tide Gauge Station in the Turkish National Sea Level Monitoring System (TUDES). According to the strategies, the highest correlation was 0.94 and the lowest mean square error was 3.76 cm. The results showed that GNSS-IR is a powerful technique capable of determining sea level changes with high precision.

Keywords: Multipath, Sea Level Change, GNSS-IR, TUDES, Tide Gauge.

Cited As:

Yalçin, G. (2023). Modeling of Sea Level Changes with GNSS-IR Method and Comparative Analysis with Tide Gauge Data, Advances in Geomatics, 1(1), 32-47. https://doi.org/10.5281/zenodo.10202317

INTRODUCTION

Sea level change is a critical indicator of climate dynamics and poses significant challenges to coastal regions worldwide. Accurate and reliable measurements of sea level variations are essential for understanding the impacts of climate change, assessing coastal vulnerability, and formulating effective adaptation strategies. While traditional sea level monitoring methods, such as tide gauges, have been widely employed, they are limited by local land movements and instrumental errors. In recent years, satellite-based remote sensing techniques have emerged as powerful tools to complement traditional approaches, providing a broader spatial coverage and overcoming many of the limitations associated with ground-based measurements. Among the satellite-based techniques, GNSS-IR has gained prominence as a promising method for studying sea level changes with high precision. GNSS-IR uses the signals transmitted by global navigation satellite systems, such as the Global Positioning System (GPS), and analyzes their reflections from various surfaces, including the sea surface. By examining the characteristics of the reflected signals, GNSS-IR enables the estimation of sea level changes with enhanced accuracy and coverage.

Several researchers highlighted the advancements and potential applications of GNSS-IR for sea surface height estimation. These studies demonstrate the feasibility and accuracy of GNSS-IR in measuring sea surface height, particularly in regions with limited altimetry coverage or complex coastal environments. The determination of environmental characteristics by analyzing reflected signals was first studied in 1993 by Martin Neira, who investigated the feasibility of determining the sea level with reflected signals from the ocean surface recorded at the receiver (Martin-Neira, 1993). Anderson (2000) established a link between the interference pattern in the recorded Signal-to-Noise Ratio (SNR) caused by the ocean-reflected signal interfering with the direct satellite signal and measurements of sea level height. Larson et al. (2013) first conducted the sea level determination according to the GNSS-IR method using GPS SNR data. Santamaría-Gómez and Watson (2017) conducted a study on the usability of high satellite elevation angle. Matthews et. al. (2020), analyzed records from over 250 GNSS receivers throughout the world to establish a worldwide archive for preserving and delivering GNSS-IR data, as well as to combine this data with current sea level observing networks in the Permanent Service for Mean Sea Level (PSMSL) data bank. They aimed to establish and/or populate controlled vocabularies with the new parameters, site identifiers, and other discovery metadata as needed. Currently, there is a need for additional improvement in the accuracy of sea level determined using GNSS single-frequency measurements. A new retrieval approach based on the peak weighting scheme of integrating the corresponding sea level retrieved from SNR data of two single frequency L1 and L2 of the GPS is proposed by Wang et al. (2020) in order to address this issue. Wang and Wang (2020) introduces the robust regression method to improve a dynamic SNR analysis based on the least square method that leads to many outliers in retrieval series. Dahl-Jensen et al. (2020) investigate the origin of sea level changes in the Thule, Greenland by comparing measured sea level

with uplift measured using GPS and modeled from height changes of the Greenland ice sheet, as well as sea surface temperatures and modeled sea level changes from gravimetry. Peng et al. (2021) study the capability of GNSS-IR to estimate coastal absolute sea-level changes and integrate on-land (coastal GNSS) and offshore (satellite altimetry) observations. Ghiasi et al. (2021) analyzed SNR data from a GPS station in Honolulu, Hawaii, over a one-month period to determine the amplitude of the major tidal constituents. They proposed that the GNSS-IR approach be used to estimate tidal constituents over a short period of time, such as one month. Dahl-Jensen et al. (2021) investigate whether GNSS-IR can be used to estimate inter-annual sea level fluctuations in Thule, Greenland, where sea ice and icebergs are present for much of the year. From 2008 through 2019, they compared annual average sea level variations using the two techniques. Beşel and Kayıkçı (2021) investigated the sea level change in Turkish seas with GNSS-IR technique and observed that the most suitable GNSS stations are MERS and TEKR stations. Altuntaş and Tunalıoğlu (2022b) analyzed the accuracy of SNR estimations by changing GNSS receiver characteristics and installations. Wei et al. (2023) provide a new GNSS-IR sea-level estimation methodology that incorporates local mean decomposition and the Lomb-Scargle periodogram.

Despite relevant literature on GNSS-IR and sea level change analysis, further research is needed to address remaining challenges and enhance the capabilities of GNSS-IR for sea level change analysis. This study aims to contribute to the existing body of knowledge by conducting an in-depth analysis of sea level changes using the GNSS-IR technique. Specifically, we utilize satellite data from the MERS station within the TUSAGA-Aktif network for the year 2021. The study focuses on analyzing the data using various strategies and validating the results against measurements from the Erdemli Tide Gauge Station within the TUDES. The subsequent sections of this article present the methodology employed in our study, the data analysis results, and the implications of our findings for sea level change monitoring and management. The outcomes of this research will contribute to advancing the understanding and application of GNSS-IR as a powerful technique for sea level change analysis, providing valuable insights for coastal regions and climate scientists.

1. METHODOLOGY

While GNSS receivers receive satellite signals from all directions simultaneously, undesired signal reflections are also encountered depending on the terrain and signal elevation angle. Most of the errors in precise position determination are caused by multipath. Multipath is when the transmitted signals reach the receiving antenna by following one or more paths. The reflectivity of the surface varies according to the satellite elevation angle, i.e. the angle of incidence of the signal. In the case of low elevation angle and high surface roughness, the signals from the satellite are weakened and reflected from the surface. Since the distance between the satellite and the receiver is much larger than the distance between the reflection surface and the receiver, it can be said that the paths of the direct and

reflected signals are parallel. In the multipath geometry shown in Figure 1, h is the vertical distance of the antenna phase center of the GNSS receiver from the reflection surface, E is the satellite elevation angle and Δs is the multipath delay.

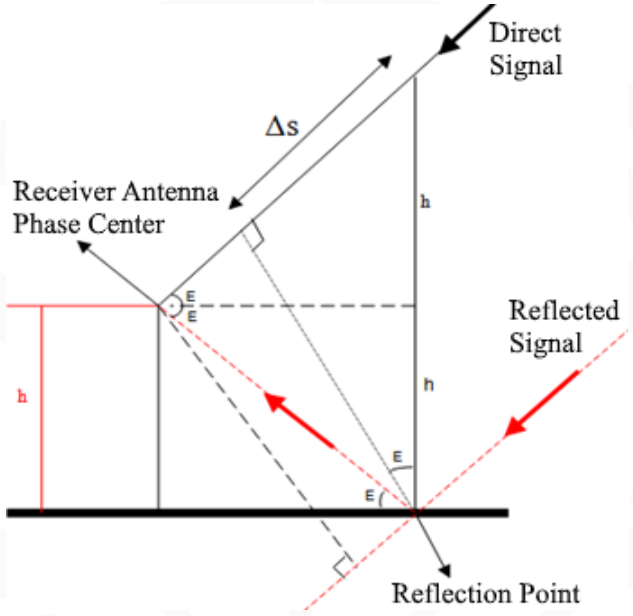

Figure 1. Multipath geometry.

GNSS-IR is a method that allows the geometric and radiometric properties of the reflection surface to be determined by modeling the oscillations caused by multipath effects in the SNR data, which indicates the strength of the GNSS signal reaching the receiver (Qian and Jin, 2016; Tabibi et al., 2017; Wang et al., 2018).

GNSS-IR allows the determination of sea level using reflected signals. The sea level is determined by measuring the vertical distance between the antenna phase center and the sea level. The direct and reflected signals received by the GNSS antenna are combined to form a composite signal, where SNR data is observed (Wang et al., 2018; Williams et al., 2020). SNR is defined as the ratio of signal power to noise power in a bandwidth.

The composite signal depends on the satellite elevation angle (E), the wavelength of the GNSS signal (λ) and the vertical distance between the antenna phase center and the reflecting surface (h, reflector height). This signal interference causes characteristic fluctuations in the SNR data. The mathematical expression of SNR is given in Eq. 1 (Bilich et al., 2007; Larson and Nievinski, 2013).

$$SNR^2 = A_c^2 = A_d^2 + A_r^2 + 2A_dA_r\cos\psi \quad (1)$$

Where A_c is the amplitude of the interfering composite signal, A_d is the amplitude of the direct signal, A_r is the amplitude of the reflected signal and ψ is the phase difference between the two signals. GNSS

receiver antennas receive direct signals more strongly than reflected signals. For this reason, direct signals contribute more to SNR values. By eliminating the contribution of direct signals, the contribution of reflected signals to SNR data can be found. The contribution of direct signals to SNR is usually in the form of a modelable trend. By applying a low-order polynomial, the effect of the direct signal is removed to obtain detrended SNR (δSNR) data. The δSNR data is obtained as given in Eq. 2 (Larson and Nievinski, 2013; Larson et al., 2013).

$$\delta SNR = A\cos\left(\frac{4\pi h}{\lambda}\right)\sin(E) + \varphi \tag{2}$$

Where A is the amplitude, h is the reflector height (vertical distance between the reflection surface and the antenna phase center), φ is the phase offset, E is the satellite elevation angle, and λ is the GNSS receiver wavelength. To calculate the reflector height, the Lomb Scargle Periodogram (LSP) (Lomb 1976; Scargle 1982) analysis is applied to the δSNR data and the dominant reflection frequency corresponding to the highest spectral power is calculated by Eq. 3.

$$f = 2h/\lambda \tag{3}$$

With this equation, the calculated frequency values of the δSNR data are converted into the vertical distance from the sea surface to the antenna phase center, i.e. the reflector height, as shown in Eq. 4.

$$h = f\lambda/2 \tag{4}$$

3. DATA AND ANALYSIS

TUDES was established to monitor sea level change in Turkey and to improve the Turkish National Vertical Control Network (TUDKA) datum and increase the reliability of elevation information. At TUDES stations, meteorological parameters (air pressure, wind, humidity, air temperature) that affect sea level changes can also be observed. TUDES consists of 20 digital and automatic tide gauge stations distributed along the coasts of Turkey and Northern Cyprus as shown in Figure 2.

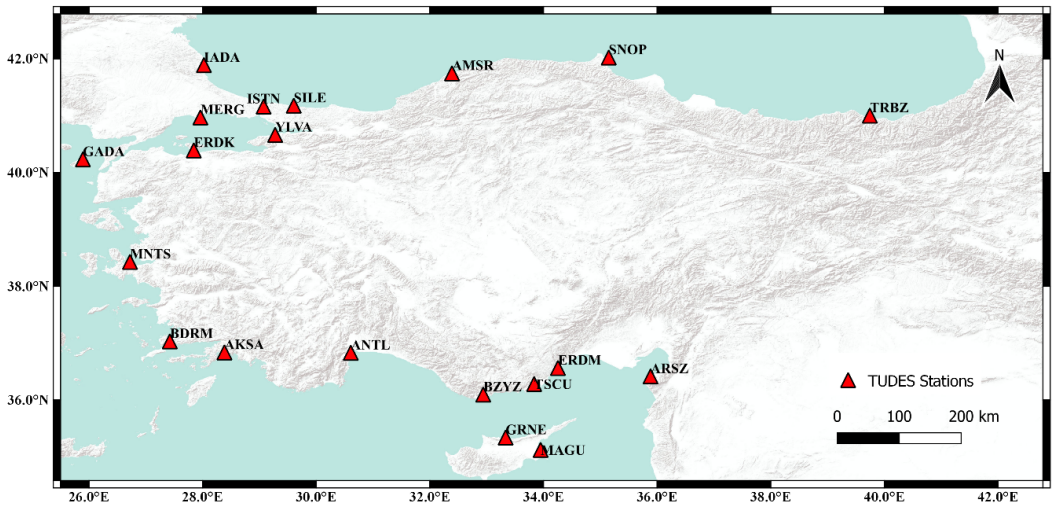

Figure 2. Map of the distribution of tide gauge stations in Turkey and Northern Cyprus.

In the study area, a GNSS station located on the seashore, which is advantageous for GNSS-IR due to its ability to capture reflections from the sea surface and a mareograph station belonging to the TUDES network was located in the same area to be used as verification data. For this purpose, the study area was selected as the coastal region of Mersin province. GNSS observation data were obtained in RINEX format. Sea level measurements of Erdemli tide gauge station belonging to the TUDES network for the year 2021 were taken in order to verify the analyzes made with the GNSS-IR method. Location information of the Erdemli tide gauge and MERS GNSS stations are given in Table 1.

Table 1. Information of Erdemli and MERS stations.

Stations	Latitude	Longitude
Erdemli tide gauge	36.56372	34.25539
MERS GNSS	36.56639	34.25585

Figure 3. Erdemli tide gauge and MERS GNSS stations.

Within the scope of this study, GIRAS (GNSS-IR Analysis System) software written in MATLAB programming language was used for data analysis (Altuntas and Tunalıoğlu, 2022a). Observation (.o) and ephemeris (.sp3) files were used in the analysis. SNR1 data of the L1 signal and SNR2 data of the L2 signal were extracted from the observation files. The sp3 files were used to calculate the satellite elevation and azimuth angle data.

The evaluation of the data takes place in two stages. First, the data is limited according to azimuth and satellite elevation angles. At this stage, care was taken to ensure that the data to be used included reflections from the sea surface and data from land areas were filtered out. This filtering can be most appropriately performed with fresnel zone analysis. The ellipsoid-shaped regions along the line of sight between the GNSS satellite and the receiver are called fresnel zones, and fresnel zones increase in direct proportion to the satellite elevation angle. As shown in Figure 4, when the fresnel zones are analyzed for the MERS station, the most suitable satellite elevation angle range for reflections from the sea surface was found to be 4°-15° and accordingly the azimuth angle range was found to be 60°-145°. The height of the MERS station above sea level is approximately 12 meters.

Figure 4. MERS station Fresnel zones according to satellite elevation angle of 4°.

The second stage of data evaluation involves the identification and elimination of outliers. Insignificant reflections are called outliers and are not used in the analysis. In this stage, background noise condition (BNC), min-max frequency filtering, and height filtering were performed.

The ratio of the spectral amplitude (peak amplitude) obtained with the δSNR data divided by the background noise is characterized by BNC, and if it is greater than a specified coefficient value, the frequency is considered useful and small reflections are meaningless and are eliminated. BNC means the average of the amplitudes other than the maximum peak amplitude. In the literature, BNC coefficients between 2-4 are used for sea level studies (Altuntas and Tunalıoğlu, 2022b). In this study, BNC coefficients of 2, 2.5, 3 and 3.5 were used.

Min-max frequency filtering is performed by calculating the mean and standard deviation of the frequencies obtained with the δSNR data, obtaining the minimum and maximum frequencies, and eliminating the estimates that are not in this frequency range.

$$f_{\max} = f_{mean} + \sigma \tag{5}$$

$$f_{\min} = f_{mean} - \sigma \tag{6}$$

Height filtering was performed by eliminating the 5% heights outside 95%, assuming that the heights calculated with Eq. 4 are normally distributed.

$$h_{\max} = h_{mean} + 2\sigma \tag{7}$$

$$h_{\min} = h_{mean} - 2\sigma \tag{8}$$

Finally, in order to estimate the sea level, the heights obtained from GNSS-IR for the first 100 days in Eq. 9 and the heights obtained from TUDES were summed and averaged (H_{mean}). Then, the reduced heights in GNSS-IR were found with Eq. 10. Figure 5 shows the workflow diagram of the analyses process.

$$H_{mean} = \frac{\sum_{i=0}^{100} h_i^{GNSSIR} + h_i^{TUDES}}{100} \qquad \text{i = 0, 1, 2,.....100} \tag{9}$$

$$h_i^{indGNSSIR} = H_{mean} - h_i^{GNSSIR} \qquad \text{i = 0, 1, 2,.....n} \tag{10}$$

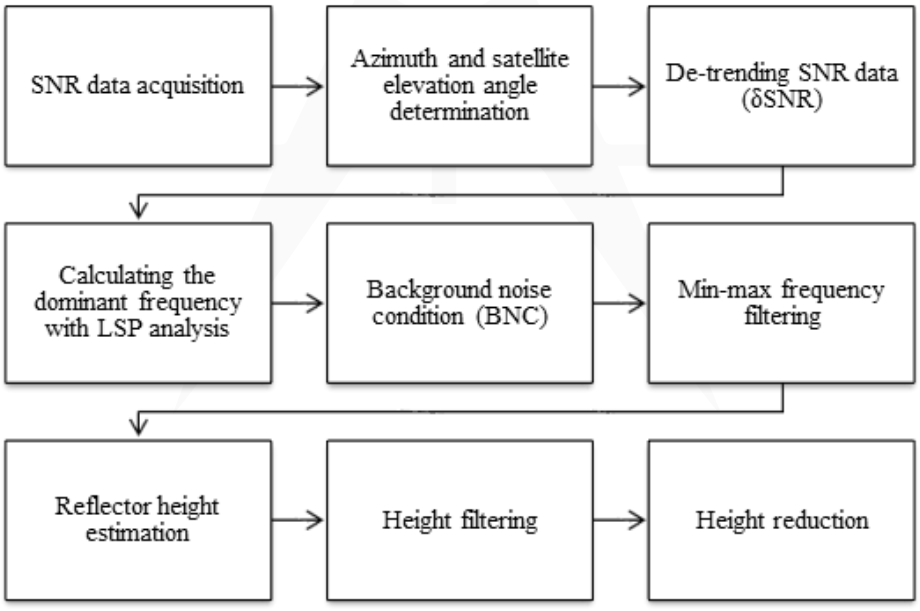

Figure 5. Workflow diagram for reflector height estimation from SNR data using GNSS-IR method.

Within the scope of the study, 16 analysis strategies with SNR1, SNR2, and SNR1&SNR2 were performed considering all cases (Table 2).

Table 2. Analysis strategies.

Strategy	Polynomial Degree	BNC	Strategy	Polynomial Degree	BNC
AS01	2	2	AS09	4	2
AS02	2	2.5	AS10	4	2.5
AS03	2	3	AS11	4	3
AS04	2	3.5	AS12	4	3.5
AS05	3	2	AS13	5	2
AS06	3	2.5	AS14	5	2.5
AS07	3	3	AS15	5	3
AS08	3	3.5	AS16	5	3.5

4. RESULTS

The pearson's correlations (r) and root mean squared errors (RMSE) obtained for each strategy as a result of the analyses are given in Table 3. Table 3 showed that the highest correlation value with SNR1 was 0.94 in the AS16 strategy. The lowest RMSE value was also found to be 3.76 cm in the AS16 strategy. Since the AS16 strategy has both the highest correlation and the lowest RMSE value, it is observed that it is the strategy that gives the best results with SNR1. The lowest correlation was obtained in AS05 and AS09 strategies with a value of 0.86. The highest RMSE value was observed in AS09 strategy with 6.21 cm. Since the RMSE value of AS05 strategy was also found to be 6.11 cm, it was observed that it provided better results in terms of RMSE than AS09. In this case, the worst results with SNR1 were obtained with the AS09 strategy. When Figure 7 is analyzed, it is observed that in the AS16 strategy, which gives the best results in SNR1, 228 days out of 297 days, i.e. 77% of them are within ±4.0 cm error.

Table 3. r and RMSE for each strategy.

Strategy	SNR1		SNR2		SNR1&SNR2	
	r	RMSE (cm)	r	RMSE (cm)	r	RMSE (cm)
AS01	0.87	6.07	0.28	28.56	0.76	8.80
AS02	0.89	5.31	0.29	28.97	0.75	8.65
AS03	0.93	4.09	0.23	36.83	0.79	7.94
AS04	0.93	4.24	0.25	49.25	0.80	7.57
AS05	0.86	6.11	0.32	26.34	0.68	10.59
AS06	0.87	5.74	0.31	26.70	0.67	10.85
AS07	0.93	4.08	0.25	33.79	0.69	10.33
AS08	0.93	4.07	0.25	46.97	0.70	10.01
AS09	0.86	6.21	0.33	25.58	0.67	10.82
AS10	0.88	5.65	0.32	26.23	0.67	10.75
AS11	0.92	4.64	0.28	33.28	0.69	10.24
AS12	0.93	4.15	0.27	45.13	0.69	10.58
AS13	0.89	5.19	0.34	24.36	0.67	10.78
AS14	0.90	4.94	0.33	25.47	0.67	10.63
AS15	0.92	4.43	0.31	29.57	0.69	10.36
AS16	0.94	3.76	0.29	40.78	0.69	10.57

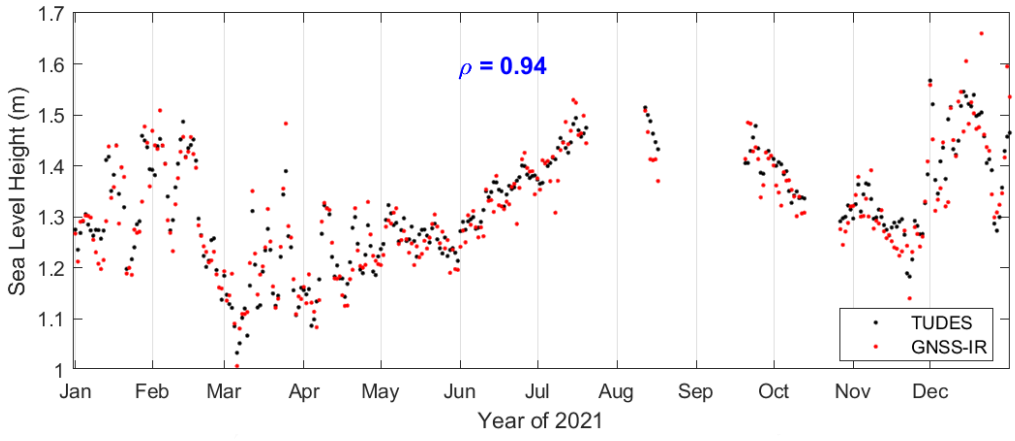

Figure 6. Sea level estimation of SNR1 data according to AS16 strategy.

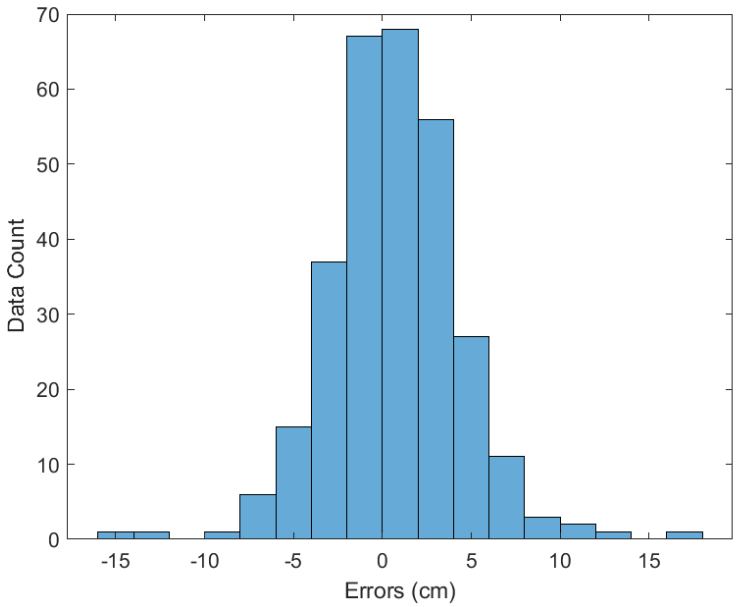

Figure 7. Error distribution of SNR1 data according to AS16 strategy.

In the analysis with SNR2 data, the highest correlation value was obtained as 0.34 in the AS13 strategy. The lowest RMSE value was obtained as 24.36 cm in the AS13 strategy. Since AS13 strategy has both the highest correlation and the lowest RMSE value, it is observed that it is the strategy that gives the best results with SNR2. The lowest correlation was obtained in the AS03 strategy with a value of 0.23. The highest RMSE value was observed in AS04 strategy with 49.25 cm. This value was found to be 36.83 cm in AS03. Since the correlation of AS04 is 0.25, it is observed that it provides a result as low as AS03 in terms of correlation. Therefore, the worst results with SNR2 were obtained with AS04. When Figure 9 is analyzed, it is observed that in the AS13 strategy, which gives the best results in SNR2, 194 days of 297 days, i.e. 65%, are within ±20.0 cm error.

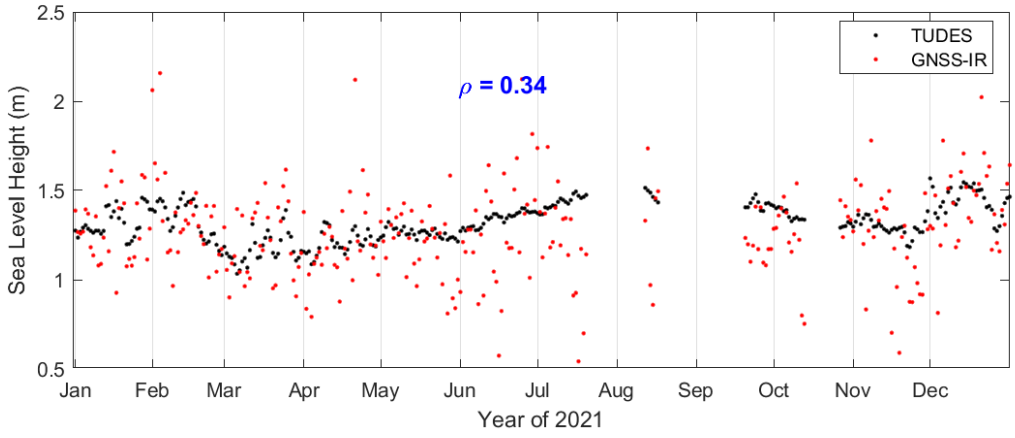

Figure 8. Sea level estimation of SNR2 data according to AS13 strategy.

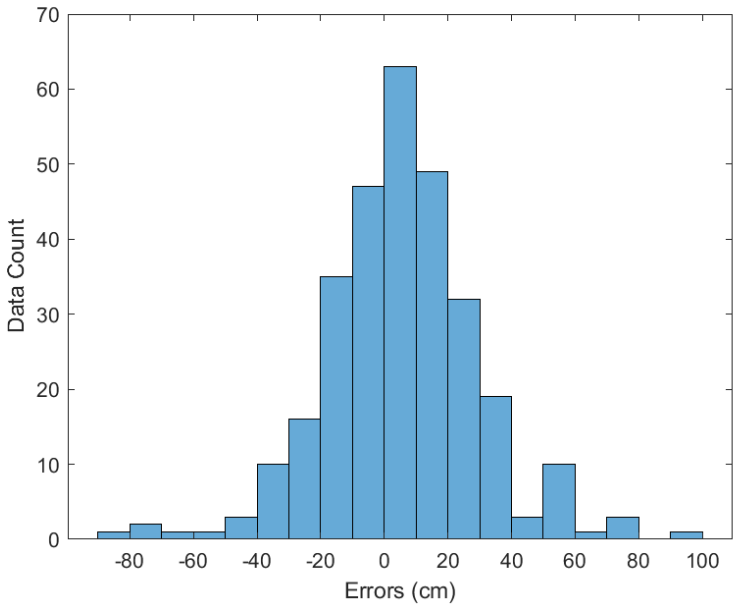

Figure 9. Error distribution of SNR2 data according to AS13 strategy.

In the analyses where SNR1 and SNR2 data were evaluated together, the highest correlation value was 0.80 in the AS04 strategy. The lowest RMSE value was also found to be 7.57 cm in the AS04 strategy. Since AS04 strategy has the highest correlation and the lowest RMSE value, it is observed that it is the strategy that gives the best results in SNR1&SNR2 analysis. The lowest correlation was observed in strategies AS06, AS09, AS10, AS13 and AS14 with a value of 0.67. The highest RMSE value was observed in AS06 strategy with 10.85 cm and AS06 strategy gave the worst result in SNR1&SNR2 analysis. When Figure 11 is analyzed, it is observed that in the AS04 strategy, where SNR1 and SNR2 data are evaluated together, 274 days out of 297 days, i.e. 92%, are within ±6.0 cm error.

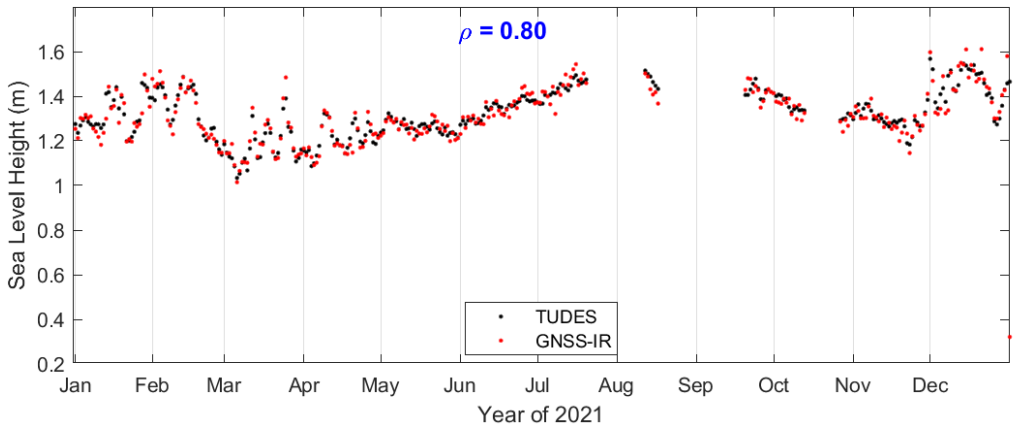

Figure 10. Sea level estimation of SNR1&SNR2 data according to AS04 strategy.

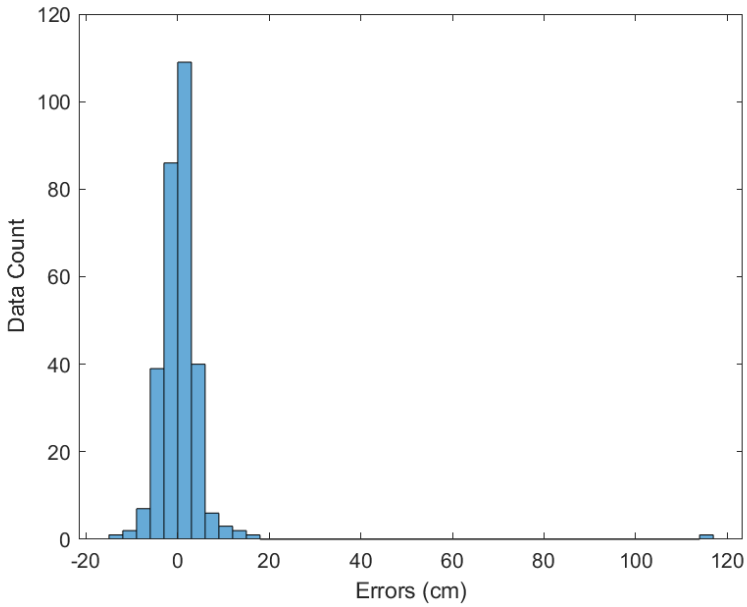

Figure 11. Error distribution of SNR1&SNR2 data according to AS04 strategy.

In general terms, when SNR1, SNR2 and both of them are analyzed together, it is observed that correlation values decrease and RMSE values increase in the analyzes performed with SNR2 data. For this reason, it can be interpreted that SNR2 data is not suitable for analysis. In the analysis with SNR1 data, it was observed that the correlation values were the highest and the RMSE values were the lowest. For this reason, it can be interpreted that SNR1 data is suitable for analysis. The lower sensitivity of SNR2 data is primarily due to the larger wavelength of the L2 signal. Because of its larger wavelength, the number of complete wave cycles within the detrended SNR segment decreases corresponding to the selected satellite elevation angle range of 4-15 degrees. This consequently leads to poorer reflector height estimations. Considering this situation, it is observed that SNR1 data is more sensitive than SNR2 data in sea level predictions.

CONCLUSIONS

In this study, to estimate the sea level in the coastal area of Mersin province with the GNSS-IR method, observation data of the MERS GNSS station located on the Mediterranean coast for 297 days in 2021 were used. The appropriate satellite elevation angle range was set to 4°-15° and azimuth angle range to 60°-145° to ensure that the reflections only come from the sea surface. The SNR data were then extracted from the observation files to obtain the δSNR data, which is free from the influence of the direct incoming signal. LSP analysis was applied to the δSNR data and the vertical distances from the sea surface to the antenna phase center were obtained with the calculated frequency values. Sea level changes obtained with 16 different strategies using polynomial degrees and background noise in different ways were compared with sea level change data from the Erdemli tide gauge station.

As a result of the 16 strategies performed, the highest correlation was 0.94 and the smallest RMSE was 3.76 cm for SNR1 data, the highest correlation was 0.34 and the smallest RMSE was 24.36 cm for SNR2 data, and the highest correlation was 0.80 and the smallest RMSE was 7.57 cm for SNR1&SNR2 data. Accordingly, the results show that the most suitable data for sea level estimation belongs to SNR1. It was observed that the use of higher order polynomials and higher BNC values slightly improved the results compared to AS16, which gave the best results in the analysis performed with SNR1 data. Previously, Beşel and Kayıkçı (2021) used SNR data of satellite tracks in the range of 60°-160° azimuth and a satellite elevation angle of 5°-20° for the MERS station. The GNSS-based sea level estimated from the MERS station was compared with the Erdemli mareograph observations. The Pearson correlation between the two observation data was calculated as 0.76. In another study, Beşel and Kayıkçı (2022) derived the dominant multipath frequency in the SNR data of the MERS station with the Lomb-Scargle periodogram (LSP) and the LSP with the Moving Average (MA) filtering. They compared the GNSS-R data of the MERS station with Erdemli tide gauge observations. For GPS L1 and L5 signals, the correlations between the GNSS-R and tide gauge using the LSP are 0.88 and 0.84. The correlations are boosted by 0.91 and 0.88 using the LSP with the MA technique.

In this study, different estimation strategies were investigated according to the polynomial degree, background noise, and SNR data. Due to the lack of certain days in the data coverage, only 297 days of 2021 were analyzed. It is recommended to use longer period data in future studies. The results of this study show that the GNSS-IR technique has significant potential for sea level monitoring. In order to use this potential to our advantage, it is very important to encourage the establishment of new GNSS stations in suitable coastal areas.

REFERENCES

Altuntas, C., & Tunalioglu, N. (2021, November). GIRAS: an open-source MATLAB-based software for GNSS-IR analysis. GPS Solutions, 26(1). https://doi.org/10.1007/s10291-021-01201-3

Altuntas, C., & Tunalioglu, N. (2022, December). Deniz seviyesi değişimlerinin belirlenmesinde GNSS-IR yönteminin kullanımı ve doğruluk analizi üzerine bir araştırma. Geomatik, 7(3), 187–196. https://doi.org/10.29128/geomatik.946594

Anderson, K. D. (2000, August). Determination of Water Level and Tides Using Interferometric Observations of GPS Signals. Journal of Atmospheric and Oceanic Technology, 17(8), 1118–1127. http://dx.doi.org/10.1175/1520-0426(2000)017<1118:dowlat>2.0.co;2

Beşel, C., & Tanır Kayıkçı, E. (2020, November). Türkiye denizlerinde GNSS reflektometre tekniği ile deniz seviyesi değişiminin araştırılması. Journal of Geodesy and Geoinformation, 8(1), 1–17. https://doi.org/10.9733/jgg.2021r0001.t

Beşel, C., & Kayıkçı, E. T. (2021, June). Determination of sea level variations in Turkish Mediterranean coast using GNSS reflectometry. Survey Review, 54(385), 310–319. https://doi.org/10.1080/00396265.2021.1939589

Bilich, A., Axelrad, P., & Larson, K. M. (2007, September). Scientific utility of the signal-to-noise ratio (SNR) reported by geodetic GPS receivers. In Proc. ION GNSS (pp. 26-28).

Dahl-Jensen, T. S., Khan, S. A., Williams, S. D., Andersen, O. B., & Ludwigsen, C. A. (2020, May). Sea level in Thule measured with tide gauge, GNSS-IR and Satellite Altimetry. In EGU General Assembly Conference Abstracts (p. 5077).

Dahl-Jensen, T. S., Andersen, O. B., Williams, S. D. P., Helm, V., & Khan, S. A. (2021, December). GNSS-IR Measurements of Inter Annual Sea Level Variations in Thule, Greenland from 2008–2019. Remote Sensing, 13(24), 5077. https://doi.org/10.3390/rs13245077

Ghiasi, Y., Farzaneh, S., Parvazi, K., & Duguay, C. R. (2021, July). Amplitue Estimation of Dominant Tidal Constituents Using Gnss Interferometric Reflectometry Technique. In 2021 IEEE International Geoscience and Remote Sensing Symposium IGARSS (pp. 8546-8549). IEEE.

Larson, K. M., Löfgren, J. S., & Haas, R. (2013, April). Coastal sea level measurements using a single geodetic GPS receiver. Advances in Space Research, 51(8), 1301–1310. https://doi.org/10.1016/j.asr.2012.04.017

Larson, K. M., & Nievinski, F. G. (2013). GPS snow sensing: results from the EarthScope Plate Boundary Observatory. GPS Solutions, 17(1), 41–52. https://doi.org/10.1007/s10291-012-0259-7

Larson, K. M., Löfgren, J. S., & Haas, R. (2013, April). Coastal sea level measurements using a single geodetic GPS receiver. Advances in Space Research, 51(8), 1301–1310. https://doi.org/10.1016/j.asr.2012.04.017

Lomb, N. R. (1976, February). Least-squares frequency analysis of unequally spaced data. Astrophysics and Space Science, 39(2), 447–462. https://doi.org/10.1007/bf00648343

Martin-Neira, M. (1993). A passive reflectometry and interferometry system (PARIS): Application to ocean altimetry. ESA journal, 17(4), 331-355.

Matthews, A., Williams, S., Bradshaw, E., Gordon, K., Hibbert, A., Jevrejeva, S., Rickards, L. & Woodworth, P. (2020, May). An International Data Centre for GNSS Interferometric Reflectometry Data for Observing Sea Level Change. In EGU General Assembly Conference Abstracts (p. 9706).

Qian, X., & Jin, S. (2016, October). Estimation of Snow Depth From GLONASS SNR and Phase-Based Multipath Reflectometry. IEEE Journal of Selected Topics in Applied Earth Observations and Remote Sensing, 9(10), 4817–4823. https://doi.org/10.1109/jstars.2016.2560763

Peng, D., Feng, L., Larson, K. M., & Hill, E. M. (2021, October). Measuring Coastal Absolute Sea-Level Changes Using GNSS Interferometric Reflectometry. Remote Sensing, 13(21), 4319. https://doi.org/10.3390/rs13214319

Santamaría-Gómez, A., & Watson, C. (2017). Remote leveling of tide gauges using GNSS reflectometry: case study at Spring Bay, Australia. GPS Solutions, 21(2), 451–459. https://doi.org/10.1007/s10291-016-0537-x

Scargle, J. D. (1982, December). Studies in astronomical time series analysis. II - Statistical aspects of spectral analysis of unevenly spaced data. The Astrophysical Journal, 263, 835. https://doi.org/10.1086/160554

Tabibi, S., Geremia-Nievinski, F., & van Dam, T. (2017, July). Statistical Comparison and Combination of GPS, GLONASS, and Multi-GNSS Multipath Reflectometry Applied to Snow Depth Retrieval. IEEE Transactions on Geoscience and Remote Sensing, 55(7), 3773–3785. https://doi.org/10.1109/tgrs.2017.2679899

Wang, X., Zhang, Q., & Zhang, S. (2018). Water levels measured with SNR using wavelet decomposition and Lomb–Scargle periodogram. GPS Solutions, 22(1). https://doi.org/10.1007/s10291-017-0684-8

Wang, J., Xu, T., Wang, N., He, Y., & Gao, F. (2020). Research on Sea Surface Height Measurement Based on GNSS-IR Dual Frequency Data Fusion. In China Satellite Navigation Conference (CSNC) 2020 Proceedings: Volume I (pp. 153-165). Springer Singapore.

Wang, X., & Wang, J. (2020, May). An Improved Height Rate Correction Method Based on Robust Regression for Sea Level Estimation in GNSS Interferometry Reflectometry. In China Satellite Navigation Conference (pp. 121-128). Singapore: Springer Singapore.

Wei, Z., Ren, C., Liang, X., Liang, Y., Yin, A., Liang, J., & Yue, W. (2023, July). Sea-Level Estimation from GNSS-IR under Loose Constraints Based on Local Mean Decomposition. Sensors, 23(14), 6540. https://doi.org/10.3390/s23146540

Williams, S. D. P., Bell, P. S., McCann, D. L., Cooke, R., & Sams, C. (2020, October). Demonstrating the Potential of Low-Cost GPS Units for the Remote Measurement of Tides and Water Levels Using Interferometric Reflectometry. Journal of Atmospheric and Oceanic Technology, 37(10), 1925–1935. https://doi.org/10.1175/jtech-d-20-0063.1